PERSPECTIVE

Weak covalent interactions and anionic charge-sharing polymerisation in cluster environments

Received 00th January 20xx, Accepted 00th January 20xx

DOI: 10.1039/x0xx00000x

Yerbolat Dauletyarov and Andrei Sanov*a

We discuss the formation of weak covalent bonds leading to anionic charge-sharing dimerisation or polymerisation in microscopic cluster environments. The covalent bonding between cluster building blocks is described in terms of coherent charge sharing, conceptualised using a coupled-monomers molecular-orbital model. The model assumes first-order separability of the inter- and intra-monomer bonding structures. Combined with a Hückel-style formalism adapted to weak covalent and solvation interactions, it offers insight into the competition between the two types of forces and illuminates the properties of the inter-monomer orbitals responsible for charge-sharing dimerisation and polymerisation. Under typical conditions, the cumulative effect of solvation obstructs the polymerisation, limiting the size of covalently bound core anions.

1 Introduction

Clusters (as known in chemistry) are microscopic systems whose structures and stability are controlled by an interplay of covalent and noncovalent interactions. 1,2 They can be viewed as aggregate entities composed of self-contained atomic or molecular moieties (monomers), which largely preserve their separate identities and internal (*intra*-monomer) bonding properties. In a cluster, these moieties are held together by *inter*-monomer interactions, which are often noncovalent in nature, but may also involve the formation of dimerising or polymerising covalent bonds.

This article offers a new look at the formation of weak (order-of-1/2 or less) covalent bonds between closed-shell monomers in anionic cluster environments. This is not a review, but a *perspective* on the topic. It exploits straightforward fundamental concepts, such as coherent charge sharing, to provide a tutorial view of covalent bonding in clusters and its competition with electrostatic solvation. Given the possibility of forming new covalent bonds with the addition of an electron, we seek to understand why one rarely observes polymer-anion cluster cores larger than a dimer. The answer could be rooted in the limits of electronic coherence, but we show that carefully constructed energetic arguments are sufficient to provide an explanation.

The following discussion is framed in the context of a Hückel-style molecular-orbital (MO) model, introduced as a simple mathematical framework for describing the inter-monomer (IM) covalent bonding and solvation trends. We touch upon some classic examples, such as the dimer anion of CO_2 , before focussing on the π - π interactions in cluster anions of organic molecules. Contrary to the noncovalent π stacking of neutral organics, the anionic π - π interactions discussed in this work are covalent in nature, as they involve an electron entering a bonding

Arizona 85721, U.S.A.; Email: sanov@arizona.edu.

MO. Broadly speaking, they are an example of charge sharing leading to covalent bond formation. We discuss the anionic π - π bonding using glyoxal and biacetyl as model systems, which possess the necessary proclivity to such interactions.⁵

In addition to covalent effects, the presence of charge in cluster anions also increases the magnitude of the noncovalent forces. The ion-neutral interactions (charge-dipole, charge-quadrupole, charge-induced dipole, etc.) are typically in the 0.1–1 eV range, compared to the 0.004–0.04 eV magnitude of the London dispersion forces between neutral atoms or molecules. In clusters, the cumulative effect of all IM forces, including the manybody interactions, needs to be considered and it is not uncommon for the overall effect of solvation to compete successfully with covalent bonding. This competition is key to understanding why charge sharing tends to be limited to just a few monomers.

To set the stage, we will consider a broad, but not exhaustive, classification of the species known as cluster anions, drilling down only on the types discussed in this Perspective. At the top, all cluster anions are divided into the homogeneous and heterogeneous types. As used in this article, these terms refer only to the identities of the monomers, the cluster building blocks. A homogeneous cluster consists of *n* identical molecular or atomic moieties X, which bind an excess electron in some fashion. The corresponding molecular formula X_n does not provide any indication of how the charge is bound to the cluster (i.e., if it is localised on a single X, shared between several X monomers, or delocalised over the entire cluster). Examples of homogeneous cluster anions include $(H_2O)_n^-$, $(CO_2)_n^-$, Ar_n^- , and O_{2n}^- , corresponding to $X = H_2O$, CO_2 , Ar, and O_2 , respectively. In contrast, a heterogeneous cluster consists of at least two types of monomers, e.g. $I^-\cdot Ar_n$, $I_2^-(CO_2)_n$, $(CO_2)_n^-\cdot (H_2O)_k$, and others.

In the ground state of a heterogeneous cluster anion, the charge naturally binds to a moiety or moieties with greater electron affinity, as in the examples above. In homogeneous clusters, all building blocks are identical and the binding of the excess electron may exhibit several distinct motifs. We will explicitly

^a Department of Chemistry and Biochemistry, The University of Arizona, Tucson,

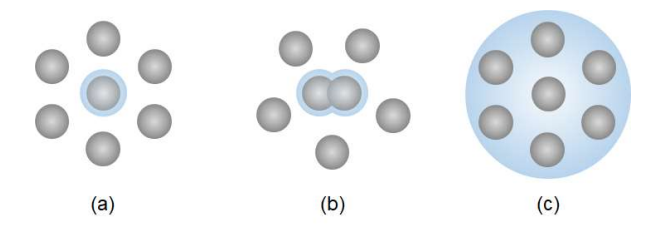


Fig. 1. (a)-(c) Schematic representations of case A, B, and C (respectively) homogeneous X_n^- cluster anions, as discussed in the text. Darker (grey) spheres represent atomic or molecular monomer moieties X, while the lighter (blue) halos represent the diffuse wave function of the excess electron.

consider three. To describe them, we will use the more informative variants of the molecular formula X_n^- , which we will refer to as structural formulas. The first motif (case A) corresponds to the excess charge localized on a single monomer, as conveyed by the structural formula X^- : X_{n-1} . The anionic moiety X^- in this case is the cluster core, while the remaining (n-1) neutral moieties are viewed as the solvent, bound to the core anion (the solute) by noncovalent (electrostatic) interactions. A generic case-A cluster is shown in Fig. 1(a), where each of the darker (grey) spheres represents an atomic or molecular monomer X, while the lighter (blue) halo around one of the monomers represents the diffuse wave function of the excess electron, bound to this monomer. An example of type-A clusters is the $(CO_2)_n^-$ series in the n=7-13 range: these clusters have CO_2^- cluster cores.^{6,7}

Alternatively (case B), the charge in X_n^- may be localised on a subset of the building blocks, as conveyed by the structural formula $X_k^- \cdot X_{n-k}$, $2 \le k \le n$. In this case, X_k^- is the cluster core, solvated by (n-k) neutral moieties. Such clusters tend to have dimer-anion cores (k=2), consisting of two covalently bound monomers sharing the excess electron, as in $(CO_2)_n^-$ with $2 \le n < 7$ and n > 13.6,7 A generic illustration of a type-B cluster, specifically for k=2, is given in Fig. 1(b). The shared electron in this case occupies an inter-monomer orbital (IMO), described as a superposition of the valence orbitals of two monomers. Such coherent electron sharing results in IM covalent bonding and the formation of a dimer anion, which is the core of the $X_2^- \cdot X_{n-2}$ cluster. Clusters with trimer-anion (k=3) or even larger cores are also conceivable, and some examples will be discussed.

In yet another class of homogeneous cluster anions (case C), the excess electron is not bound to any specific monomer(s). Instead, it is localized in a solvent cavity or delocalized over the surface or the bulk of the cluster. The last case is illustrated in Fig. 1(c). To be clear, case-C clusters do not correspond to the k = n limit of case B. In case C, the excess electron does not enter the valence orbitals of the monomers and does not form covalent IM bonds. A case-C scenario may occur when the lowest vacant orbital of X is high in energy, preventing the formation of valence X^- or X_k^- anions. In a case-C cluster, there is no core anion, unless one considers the electron itself as the cluster core. The famous example of type-C species are the hydrated-electron clusters $(H_2O)_n$ -.8-21

From this point on, we will focus on the homogeneous case-A and case-B clusters, $X_k \bar{\ } X_{n-k}$, $1 \le k \le n$. Among these, we will zero in on species with the dimer- or polymer-anion cores, which consist of closed-shell (in the neutral state) monomers bound

together *only* as a result of electron attachment. In such cases, the neutral monomers interact via the van der Waals forces, while the X_k^- core anion is formed due to an electron entering a bonding IMO (which is vacant in the neutral state). The reverse process causes X_k^- to fall apart to k unbound X moieties: $X_k^- \to k X + e^-$ (dissociative detachment).^{22,23} This scenario plays out, for example, in the $(CO_2)_2^-$ dimer, where the excess electron populates a bonding superposition of the two CO_2 s lowest-unoccupied orbitals.³ We will refer to such phenomena as *anionic charge-sharing polymerisation*, and it is this type of anions that is the focus of this Perspective. Such IM bond formation is the result of coherent charge-sharing. It is distinct from anionic addition chain-growth polymerisation, which is initiated by anions and involves the propagation of a *localised* negative charge.²⁴

The bonding modalities in cluster anions can be elucidated by photoelectron spectroscopy. Solvated anions are strongly stabilized by ion-neutral interactions, while the neutral states are hardly affected, due to the relative weakness of the van der Waals forces. Anion solvation, therefore, results in observable shifts of the photodetachment transitions to progressively larger electron binding energies (eBE), as the cluster size increases. In the absence of chemical rearrangements, the increase in eBE with the cluster size is monotonic and gradual. Any discontinuities in the trend signal changes in the core anion structure. 1,2

Abrupt changes in the core anion properties upon the addition of solvent molecules are often referred to as "core switching". Many reports are available in the literature, with the classic example being the $(CO_2)_n$ - series.^{6,7} For n = 2-6 and n > 13, these clusters have covalent dimer³ cores, (CO₂)₂⁻ or C₂O₄⁻, while in the n = 6-13 range, the core structure switches to the CO_2^- monomer. Since C₂O₄⁻ and CO₂⁻ have markedly different properties, they are clearly distinguishable in the photoelectron spectra of size-selected $(CO_2)_{n}^{-0.6,7}$ In other cluster series, the size-dependent change from one core type to another may be less abrupt. Such clusters exhibit the coexistence of core types over a range of n, and it is more appropriate to describe the gradual change as core-shifting (rather than core-switching).²⁵ Examples of coexisting monomer- and dimer-anion cores include the (OCS)_n- and $(CS_2)_n$ clusters. ²⁶⁻³⁹ Similarly, the heterogeneous $O^-(N_2O)_n$ series also exhibits the coexistence and a gradual shift between the $O^-(N_2O)_n$ and $NNO_2^-(N_2O)_{n-1}$ structures.⁴⁰⁻⁴²

The question of why certain core types are favoured in the presence of fewer solvent molecules, while others gain ground when the cluster size is increased, is central to cluster chemistry. Sometimes the key lies in reaction dynamics and/or the cluster formation mechanism, but under the conditions of thermodynamic equilibrium it comes down to the relative stabilities and free energies. We will consider these trends by focusing on the homogeneous cluster anions with the generic molecular formula X_n -and discuss the factors that promote or obstruct the charge-sharing polymerisation and control the stabilities of the isomers described as $X \cdot X_{n-1}$, $X_2 \cdot X_{n-2}$, ..., $X_k \cdot X_{n-k}$, ..., $k \le n$.

Uncommon acronyms used in this article:

MMO MonoMer Orbital. Used instead of MO (molecular orbital) to distinguish between the orbitals of a monomer X and those of the cluster X_n . Symbol ψ is used for the MMOs throughout. HOMMO and LUMMO are the

Highest-Occupied and Lowest-Unoccupied MMOs. The HOMMO and LUMMO of a specific monomer $X^{(i)}$ are $\psi^{(i)}_{\text{HOMMO}}$ and $\psi^{(i)}_{\text{LUMMO}}$, respectively.

IM Inter-monomer.

IMO Inter-monomer orbital—a cluster MO, defined as a linear combination of the MMOs of two or more monomers. Symbol ϕ is used for the IMOs throughout.

LCMO Linear combination of molecular orbitals, as opposed to the linear combinations of atomic orbitals (LCAO) in the LCAO-MO theory.

CMMO Coupled-Monomers MO model.

VSE Vertical Stabilisation Energy. The combined energy of IM interactions within the cluster, including both covalent and electrostatic forces, but excluding the relaxation energy of the monomers. Defined to be positive.

CSE Cluster Stabilization Energy. The overall stabilization energy of X_n^- relative to the relaxed $X^- + (n-1)X$ dissociation limit. Defined as a positive value.

2 Covalent and solvation interactions in clusters

On a pairwise basis, the noncovalent interactions implicated in solvation are usually weaker than the chemical bonds in either the solute or the solvent. However, the cumulative effect of solvation, including the many-body interactions, ⁴³ in a large enough cluster can exceed the energy of a covalent bond, especially if the bond in question is weak. We will discuss anionic charge-sharing polymerisation due to the formation of covalent bonds between the monomer building blocks of a cluster. The formation of such bonds may be impeded by the solvent, i.e., sacrificed in favour of maximising the noncovalent solvation interactions.

The electrostatic interactions within the first solvation shell generally favour smaller cluster cores. Comparing the monomervs. dimer-anion based clusters, the monomer anions, due to their smaller size and, therefore, more localised charge, interact more strongly with the nearest solvent molecules. In other words, solvation is more favourable in the monomer-based $X^- \cdot X_{n-1}$ clusters compared to the dimer or polymer-based counterparts, $X_k^- \cdot X_{n-k}$, $k \geq 2$. This sets up a thermodynamic mechanism for the solvation impeding the formation of dimer or polymer anions, illustrated by the schematic energy diagram in Fig. 2.

The diagram reflects the competition between the covalent and solvation interactions in the dimer- vs. monomer- based clusters: $X_2^- \cdot X_{n-2}$ (left) vs. $X^- \cdot X_{n-1}$ (right). It accounts for IM interactions only, so that the isolated monomer anion X^- corresponds to the zero of energy (no IM interactions). Upon the addition of a second X moiety, one of two basic species can form: a covalent dimer anion X_2^- (left) or the ion-molecule complex $X^- \cdot X$ (right). The dimer dissociation energy, $D_0(X_2^-)$, is usually larger than the solvation magnitude in the ion-molecule complex, $|\sigma_{1,1}|$. Note that while $D_0(X_2^-)$ is positive, $\sigma_{1,1}$ and other similar solvation factors used in this work are defined to be negative.

The addition of a third X moiety to either X_2^- or X^- ·X leads to further stabilisation of either X_2^- ·X or X^- ·X₂ (covalent trimer anions X_3^- and larger polymers are not included in Fig. 2; they will be discussed later). The solvation interaction in X_2^- ·X, $\sigma_{2,1}$,

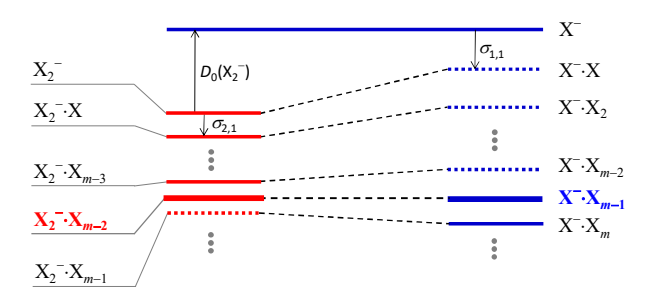


Fig. 2. Schematic diagram illustrating the thermodynamics of core-switching/ shifting from the $X_2^- X_{n-2}$ to $X^- X_{n-1}$ cluster structures. Solid levels correspond to the preferred isomers for each cluster size n, while the dashed levels represent metastable structures. Although the X_2^- covalently bound dimer anion is assumed to be more stable than the $X^- X$ ion-molecule complex, the more efficient solvation of the monomer leads to an approximate degeneracy of the $X_2^- X_{m-2}$ and $X^- X_{m-1}$ cluster isomers for certain cluster size m. For the X_n^- clusters with n < m, the dimer-based structures are favoured energetically, while for n > m the monomer-based isomers are preferred.

is expected to be weaker than each of the pairwise X^-X interactions in X^-X_2 , because of the smaller charge density in the dimer-based cluster. As a result, the difference between X_2^-X and X^-X_2 is smaller than that between X_2^- and X^-X .

This trend will usually continue with the addition of more X moieties, at least until the first solvation shell is filled. Since every solvent moiety added to a monomer-based cluster stabilises it by more than a similar molecule added to a dimer-based cluster, there will exist a size m for which the dimer and monomer-based structures $X_2^- \cdot X_{m-2}$ and $X^- \cdot X_{m-1}$ have similar energies, as represented by the isoenergetic (bolded) levels in Fig. 2.

The $(CO_2)_n^-$ cluster series is a classic example of this behaviour. 6,7 In the n=2-5 range, the formation of an anionic order-of-1/2 covalent bond between two CO_2 moieties³ favours the $(CO_2)_2^-(CO_2)_{n-2}$ structures. However, already for n=6, coexisting $(CO_2)_2^-(CO_2)_4$ and $CO_2^-(CO_2)_5$ structures are observed. $^{6,7,44-46}$ This means that even though the $(CO_2)_2^-$ dimer anion is more stable than the $CO_2^ CO_2$ ion-molecule complex, the combined effect of forming the covalent IM bond and solvating the dimer with four CO_2 's is approximately the same as that of solvating the monomer anion CO_2^- by five CO_2 's.

The photoelectron spectra of size-selected $(CO_2)_n^-$ display two band series: one, corresponding to higher vertical detachment energies (VDE), is observed for the n = 2-6 and $n \ge 14$ clusters, and the other, with lower VDEs, in the n = 6-13 range.^{6,7} The discontinuities at n = 6 and 14 cannot be accounted for by solvation and are attributed to structural changes in the cluster cores. These changes have been described as core-switching from the covalent dimer anion, whose D_{2d} symmetry structure was originally proposed by Fleischman and Jordan,³ to the CO_2 -monomer at n = 6 and back to the dimer at n = 14.^{6,7} The reverse core-switching at n = 14 is attributed to the completion of the first solvation shell in $(CO_2)_2$ - $(CO_2)_{12}$.

Tsukuda et al.⁴⁷ reported a similar phenomenon for $(NO)_n^{-1}$. For this series, the VDE was found to increase by ~2.4 eV from n = 1 to n = 2 and by nearly 0.8 eV from n = 2 to n = 3, while only moderate consecutive increases (~0.1–0.2 eV) occur in the n = 3-7 range. The n = 3-7 trend for is consistent with stepwise

solvation of a charged cluster core, but the abrupt changes between n=1 and 2 and between n=2 and 3 signal structural changes in the core anion. The n=1 species is NO⁻; n=2 is a covalently bound dimer anion (NO)₂⁻, for which several isomeric forms have been proposed. $^{40,48-53}$ The n=3 cluster is (preferentially) a covalent trimer, (NO)₃⁻. That is, in the n=1-3 range, the excess electron in (NO)_n⁻ is shared between all available NO moieties. In larger clusters, however, further polymerisation is impeded by solvation and the size of the core anion no longer increases with n. 47 This brings us back to the question of why, once again (as in many other examples), electron binding is limited to just 1-3 cluster building blocks.

3 Anionic dimerisation

3.1 General types of covalent dimer anions

We begin the discussion of anionic polymerisation in case-B clusters [Fig. 1(b)] with the covalent dimer anions X_2^- , in which the charge is coherently shared between the two monomers. For such dimer anions, we identify three possible electronic motifs:

Type I: Dimers with weak (order-of-1/2) IM bonds formed via anionic dimerisation of closed-shell monomers.

Type II: Dimer anions of radicals or diradicals.

Type III: Dimer anions of closed-shell molecules involving singlet-triplet excitation of the monomers.

The focus of this Perspective is on type-I species, and so it is important to distinguish these dimers from the other two motifs. The IM bonding in each type can be understood by considering the overlap of the monomer orbitals, leading to the formation of the bonding and antibonding IMO pairs, the same way as linear combinations of atomic orbitals yield molecular orbitals within the LCAO-MO theory framework. We will use the acronym MMO for MonoMer Orbitals, to set them apart from MOs (molecular orbitals), in general. Depending on the nature of X, an MMO can be either a molecular or atomic orbital.

The key feature of type-I dimerisation is that the IM bond in X_2^- forms due to the excess electron populating a bonding IMO. For example, there is no covalent bonding between the two CO₂s in the (CO₂)₂ van der Waals dimer, but in (CO₂)₂-,³ the excess electron enters an IMO described as a bonding superposition of the lowest-unoccupied orbitals of the two monomers.³³ As will be shown shortly, the resulting electron configuration yields an order-of-1/2 IM bond, which is typical of type-I dimer anions.

Type-II dimers involve the anionic pairing of neutral radicals or diradicals. Contrary to type-I cases, the IM bonding in type-II dimers is not always due to the excess electron. Because radicals and diradicals often dimerise in the neutral state, many (but not all) type-II dimer anions are best thought of as products of electron capture by neutral molecules. For example, F_2^- is (technically) a type-II dimer anion of atomic fluorine. Similarly, the anion of fumaronitrile (fn) is a type-II dimer anion of cyanocarbene, because the fn molecule, N=C-C(H)=C(H)-C=N, can be viewed as a covalent dimer of HCCN, which is a triplet-ground-state⁵⁴ diradical. Since the neutral dimer molecules already have covalent bonds between the monomers, the IM bond orders in the corresponding dimer anions can be greater than 1/2. For

example, it is 1/2 in F₂⁻, but 1.5 in fn⁻: the IM (C=C) bond order in neutral fn is 2, but the IMO occupied by the excess electron is antibonding with respect to this bond. Because of the pre-existing neutral bonds, one usually does not think about such anions as products of *anionic* dimerisation per se, as no charge is required for the dimerisation to occurs. However, there is no contradiction in the term, and in some cases (e.g., O₄⁻), ⁵⁵⁻⁶⁰ the IM bond formation indeed occurs in the anion state.

Concluding the overview, type-III dimerisation pairs monomers, which are closed-shell singlets in their ground states, but yield dimer anions whose neutral core configurations result from singlet coupling of the monomers promoted to their respective triplet states. That is, the neutral dimer configurations are doubly excited. This is not meant to imply that for type-III dimer anions to form, the neutral monomers must first undergo singlet-triplet excitations. The more straightforward pathway usually involves the anionic dimerisation of singlet monomers (a type-I process), followed by internal conversion to the doubly excited (and yet, more favourable) configurations in the anion state. Regardless of the mechanistic details, the language of double excitations is valuable, because it provides a clear depiction of the electronic structures of these species.

Examples of type-III dimers include certain states of (OCS)2and $(CS_2)_{2^-,27,28,30,31,33,36,37}$ as well as the dimer anion of fn, (fn)₂^{-.61} Fumaronitrile has a special distinction: while its monomer anion fn⁻ can be viewed as a type-II dimer of cyanocarbene (see above), (fn)₂⁻ is a type-III species.⁶¹ The distinction between the electronic motifs of $(OCS)_2^-$ and $(CS_2)_2^-,^{27,33,36}$ on the one hand, and (CO₂)₂-,³ on the other, is also striking, considering the isovalency of OCS, CS2, and CO2. The origin of this distinction is the singlet-triplet gaps in OCS (~ 3.4 eV) and CS₂ (~ 3.2 eV) vs. CO_2 (~ 5.3 eV).^{27,36} The OCS and CS_2 gaps are sufficiently small for the singlet-triplet excitation energy of two monomers to be recovered through the IM covalent bonding and the large electron affinities of the dimers (type-III anionic dimerisation). In (CO₂)₂-, the price of promoting two CO₂'s to the triplet state is too high and the most stable (CO₂)₂⁻ structure³ results from the addition of an electron to the lowest unoccupied IMO of the van der Waals dimer configuration (type-I dimerisation).

Having identified three possible electronic motifs in covalent dimer anions, we will proceed with the detailed description of type-I dimers, which are the focus of this Perspective.

3.2 Covalent dimer anions of closed-shell monomers

In type-I dimerisation, the IM bond is the result of electron capture by a bonding superposition of the lowest-unoccupied MMOs of the two monomers. The feasibility of such process depends on the availability of low-lying vacant MMOs and the relative stabilisation energy (the bond integral) of the IMO. Besides (CO₂)₂-,6,7,33,62 other pertinent examples, to be discussed here, are the dimer-anions of glyoxal and biacetyl. As an illuminating counterexample, a covalently bound dimer anion of Helium, He₂-, *would* be a type-I dimer, had it existed as a stable species. It does not, due to the lack of low-lying vacant MMOs: the 2s orbital of He is too high in energy for the excitation to be recovered by bond formation.

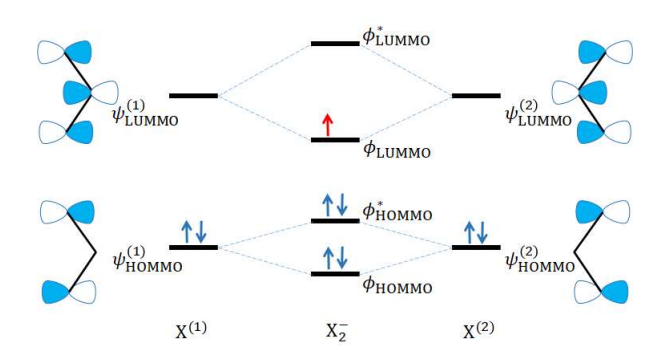


Fig. 3. Generic IMO diagram for type-I anionic dimerisation. The MMO sketches correspond to $X = \text{CO}_2$ at a bent anion geometry.

In general, consider two neutral closed-shell monomers X, identified as $X^{(1)}$ and $X^{(2)}$, each with an electron configuration:

$$X^{(i)}(Singlet): ... (\psi_{HOMMO}^{(i)})^2 (\psi_{LUMMO}^{(i)})^0$$
 (1)

 $\psi^{(i)}_{\text{HOMMO}}$ and $\psi^{(i)}_{\text{LUMMO}}$ are the highest-occupied and lowest-unoccupied MMOs (HOMMO and LUMMO) of $X^{(i)}$, i=1,2. For reference, the configuration of the valence monomer anion X^- is:

$$(X^{-})^{(i)} : ... (\psi_{HOMMO}^{(i)})^{2} (\psi_{LIIMMO}^{(i)})^{1}$$
 (2)

The general case of type-I dimerisation is illustrated in Fig. 3, where the MMO sketches correspond to $X = CO_2$. The overlap of the respective HOMMOs and LUMMOs yields pairs of bonding and antibonding IMOs, defined as:

$$\phi_{\text{HOMMO}}^{(\pm)} = \psi_{\text{HOMMO}}^{(1)} \pm \psi_{\text{HOMMO}}^{(2)} \tag{3}$$

$$\phi_{\text{LIJMMO}}^{(\pm)} = \psi_{\text{LIJMMO}}^{(1)} \pm \psi_{\text{LIJMMO}}^{(2)} \tag{4}$$

With ψ reserved for the monomer orbitals, ϕ will be used to denote the IMOs.

Normalisation factors are omitted in Eqs. (3) and (4), while the \pm signs allow for the formation of the bonding or antibonding IMO pairs. As in the LCAO-MO theory, the IMO bonding character depends not only on the sign of the superposition, but also the relative symmetry of the MMOs. Given the specific MMO sketches in Fig. 3, $\phi_{\rm HOMMO}^{(+)}$ and $\phi_{\rm LUMMO}^{(+)}$ are the bonding IMOs, but in other scenarios the minus signs can result in bonding superpositions. To avoid ambiguity, we will drop the \pm notation and use the conventional asterisk or lack thereof, respectively, to denote the antibonding and bonding IMOs. With that, based on the IMO diagram in Fig. 3, the electron configuration of a type-I dimer anion, is written as:

$$X_2^-: ... (\phi_{HOMMO})^2 (\phi_{HOMMO}^*)^2 (\phi_{LUMMO})^1$$
 (5)

This configuration corresponds to an order-of-1/2 dimerising bond, which is entirely due to the excess electron (red arrow in Fig. 3) populating ϕ_{LUMMO} . The bond disappears (its order is reduced to zero) if the electron is removed.

While the MMO sketches in Fig. 3 correspond to $X = CO_2$, the diagram itself is quite general and applies to numerous other systems. In what follows, we will use the IMO framework to describe the anionic π -stacking of glyoxal and biacetyl. This

analysis builds on other variants^{63,64} of the general MO theory. In particular, we follow in the footsteps of Krylov and co-authors, who used a similar approach (adapted to electron removal rather than addition) to investigate the bonding patterns in dimer cations of benzene,⁶⁵ uracil,⁶⁶ adenine and thymine.⁶⁷ As a side note, the diffuse nature of anion orbitals may contribute, in comparison, to the greater ease of charge sharing (delocalisation) in anionic clusters, especially beyond the dimers.

Krylov and co-authors fittingly named their theory dimer MO—linear combination of fragment MOs (DMO-LCFMO),⁶⁵ and it is only because our discussion extends beyond dimers that we use the more general term IMO instead of DMO. Moreover, as the overall formalism detailed in Sec. 4 includes both covalent and solvation interactions, we term it the coupled-monomers MO (CMMO) model. In contrast to LCAO/LCMO/LCFMO, the name emphasises the physical effect of monomer coupling (via whatever interactions are important) over the mathematical formalism of linear combinations. For example, a similar approach to coupled fragments (instead of monomers) was recently used to describe diradical interactions in bond breaking.⁶⁸

Turning to glyoxal (gl) and biacetyl (ba), the bonding IMOs of the dimer anions (as well as the corresponding trimers and tetramers) are shown in Fig. 4. They were calculated using the methodology described in Sec. 5.1 and used previously for biacetyl.⁵ The IM distances indicated for these structures are defined as the separations between the centres of the middle C–C bonds in each monomer. All other geometric details are given in Electronic Supplementary Information. The (gl)2⁻ and (ba)2⁻ IMOs in Fig. 4 can each be viewed as a superposition of the LUMMOs ($\psi_{\text{LUMMO}}^{(I)}$, i = 1, 2) of the corresponding monomers, as indicated by Eq. (4). The gl and ba LUMMOs correspond to the respective gl⁻ and ba⁻ HOMMOs, shown at the top of Fig. 4. Envisage combining one of these MMOs with its own reflection in a plane below, rotated about the vertical axis by some degree, and the result is a close approximation to the corresponding dimer IMO.

The IMO approach to covalent dimers can be easily extended to type-I trimers, tetramers, and beyond (Sec. 4), but it is important to keep in mind some of the model limitations. First, the IMO diagrams, such as Fig. 3, do not account for electron correlation and the complexities of systems with multi-configurational wavefunctions. Second, the model, as presented, attempts to separate IM bonding from the bonding structures of the monomers themselves. This is formally justified only if the inter- and intra-monomer bonds are decoupled, as in the case of the IMOs are formed from nonbonding MMOs. For the IMOs formed from orbitals involved in intra-monomer bonding, the model amounts to a first-order perturbative approach, justified only if the IM interactions are significantly weaker than the intra-monomer bonds. This requirement is satisfied in type-I dimer/polymer anions, because of the weakness of the IM bonds in these systems. In systems with stronger IM bonds (e.g., type-II and type-III dimers), the MMOs contributing to IM bonding may also be responsible for the bonds within the monomers. As strong IM bonding affects the electronic wavefunctions of the monomers, it may alter the intra-monomer bonding structures. In that case, treating the IM bonding as a first-order perturbation of the intramonomer bonds may no longer be justified.

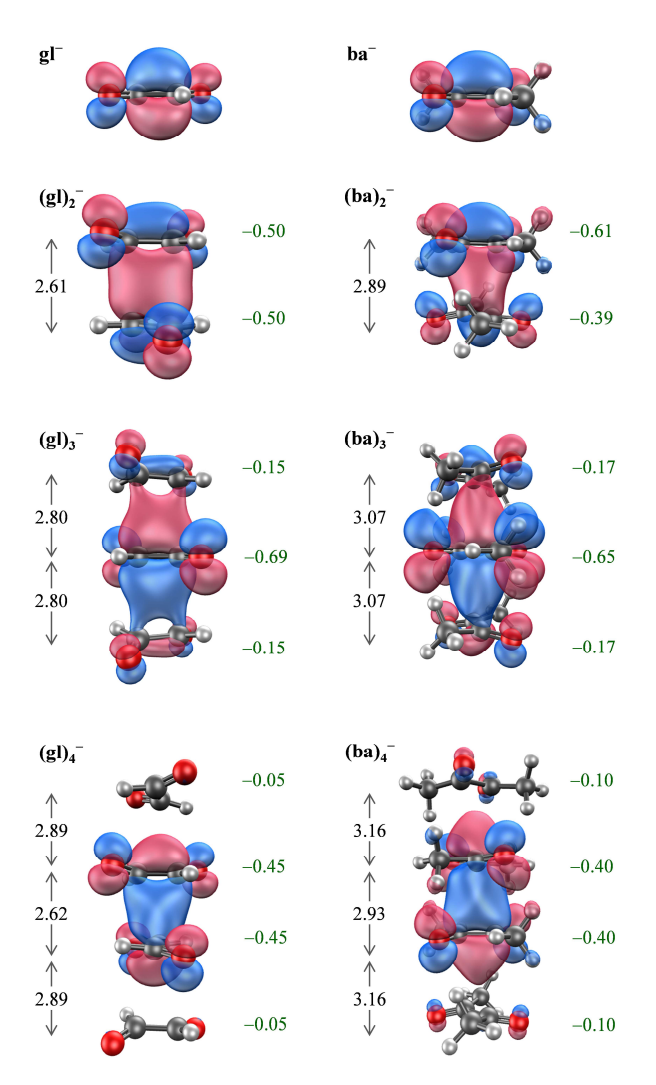


Fig. 4. The π character orbitals populated by radical electrons in the equilibrium (gl)_n⁻ and (ba)_n⁻, n = 1-4 structures. Values to the left of each structure are the IM distances (in Angstroms), measured between the centres of the (middle) C–C bonds in the respective monomer moieties. To the right are the overall Hirshfeld-I charges of each gl or ba moiety.

4 Anionic polymerisation vs. solvation in clusters

We now turn to a quantitative description of type-I polymerisation in cluster anions with the general molecular formula X_n^- and the structural formulas $X_k^- \cdot X_{n-k}$, $1 \le k \le n$. Clusters with k=1 correspond to case A, represented in Fig. 1(a), while clusters with $k \ge 2$ correspond to case B, illustrated (for k=2) in Fig. 1(b). Our goal is to combine the MO treatment of covalent interactions with the effect of electrostatic solvation and quantify the factors controlling the relative stabilities of clusters with the monomer (k=1), dimer (k=2), and polymer $(k \ge 3)$ anion cores.

4.1 Dimer anions of closed-shell molecules (n = 2)

 X_2 : Covalent dimer anions (n = 2, k = 2). Consider an anionic bond between two monomers that are closed-shell

species in their neutral states. As discussed in Sec. 3.2, the order-of-1/2 dimerising bond results from a bonding superposition of vacant MMOs, populated by an electron in the anion state (Fig. 3). This type of bonding can be described by a Hückel-style Hamiltonian matrix, defined in the basis of the MMOs responsible for the IM bond formation:

$$\mathbf{H} = \begin{pmatrix} \alpha + \sigma_{2,0} & \beta_{1/2} \\ \beta_{1/2} & \alpha + \sigma_{2,0} \end{pmatrix} = \begin{pmatrix} \alpha & \beta_{1/2} \\ \beta_{1/2} & \alpha \end{pmatrix}$$
(6)

Here, α and $\beta_{1/2}$ are the usual Coulomb and bond integrals: $\alpha = \langle \psi_i | \hat{H} | \psi_i \rangle$, $\beta_{1/2} = \langle \psi_i | \hat{H} | \psi_j \rangle$, where $\psi_i = \psi_{\rm LUMMO}^{(i)}$ are the basis MMOs and $i, j = 1, 2, i \neq j$ are the monomer indices. The gl and ba MMOs are shown at the top of Fig. 4. The Coulomb integral α corresponds to the MMO energy, while the bond integral $\beta_{1/2}$ describes the formation of the dimer IMO. The subscript indicates an order-of-1/2 IM bond, but the discussion of the bond order effect on the integral value will follow in Sec. 4.2. The quantity $\sigma_{2,0}$ in the first part of Eq. (6) is a specific case of the general solvation factor $\sigma_{k,n-k}$, defined as the total energy of electrostatic solvation of the X_k core by n-k solvent moieties within the X_k - X_k - X_k - X_k -cluster. In the absence of solvent, as for k=2 and k=0, k=0, k=0, and introduced in Eq. (6) only for completeness.

The eigenvalues of **H** in Eq. (6), $E_{1,2} = \alpha \pm \beta_{1/2}$, are the dimer IMO energies. The corresponding eigenvectors contain the coefficients representing the IMOs in the MMO basis, as described by Eq. (4). Only one electron populates the IMO system described by Eq. (6) in a type-I dimer anion. Assuming that the IM bonding is due to the stabilisation of the radical electron relative to the monomer orbitals, the bond strength is the difference between α and the smallest IMO eigenvalue, $E_1 = \alpha + \beta_{1/2}$. The bond energy is therefore $-\beta_{1/2}$, where the minus sign accounts for the negative value of $\beta_{1/2}$. This bond energy is the total of all IM interactions in X_2 . Since it does not include the vibrational relaxation of the monomers, it corresponds to *vertical* stabilisation energy, VSE = $-\beta_{1/2}$. This result is included in Table 1, summarising the VSE values of the clusters modelled in this section.

Similar to bond energies, VSE is defined to be positive for attractive interactions. The cluster stability is defined not only by the IM interactions, but also by how these interactions affect the intra-monomer structures. Hence, we will also consider the cluster stabilisation energy (CSE), defined as the difference between the relaxed $X^- + (n-1)X$ limit and the X_n^- cluster. CSE is the adiabatic counterpart of VSE, including the monomer relaxation, $\Delta E_{\rm rel}$. As illustrated in Fig. 5, CSE = VSE – $\Delta E_{\rm rel}$. As the CMMO model separates the inter- and intra-monomer interactions, we do not consider $\Delta E_{\rm rel}$ in this section; it will be included in Sec. 5.

The normalized eigenvector for the lowest eigenvalue of **H** in Eq. (6) is $(1/\sqrt{2}, 1/\sqrt{2})$. It reflects equal contributions of the MMOs, $\psi_1 = \psi_{\text{LUMMO}}^{(1)}$ and $\psi_2 = \psi_{\text{LUMMO}}^{(2)}$, to the bonding IMO, ϕ_{LUMMO} , and an even, -0.50/-0.50, charge sharing between the monomers. This is consistent with the properties of $(\text{CO}_2)_2^{-3}$ the stacked $(\text{gl})_2^{-}$ structure, and its IMO shown in Fig. 4. A slight deviation from an even distribution was previously predicted for $(\text{ba})_2^{-}$, due to the two biacetyl moieties adopting slightly different geometries.⁵

 X^-X : An ion-molecule complex (n = 2, k = 1). No covalent

Cluster size	Size of the core anion (k)						
(n)	1	2	3	4			
1	0	n/a	n/a	n/a			
2	$-\sigma_{1,1}$	$-eta_{1/2}$	n/a	n/a			
3	$-\sigma_{1.2}$	$-(\beta_{1/2} + \sigma_{2,1})$	$-1.41\beta_{1/4}$	n/a			
4	$-\sigma_{1,3}$	$-(\beta_{1/2} + \sigma_{2,2})$	$-(1.41\beta_{1/4} + \sigma_{3,1})$	$-1.62\beta_{1/6}$			

^{*} The factors of 1.41 and 1.62 appearing in the table are the approximate values of $\sqrt{2}$ and $(\sqrt{5}+1)/2$, respectively.

bond between the two monomers is present in the X^-X cluster anion, which is held together by electrostatic forces. The Hückelstyle Hamiltonian matrix for such a species is written as:

$$\mathbf{H} = \begin{pmatrix} \alpha + \sigma_{1,1} & 0 \\ 0 & \alpha + \sigma_{1,1} \end{pmatrix} \tag{7}$$

With no IM bonding, the off-diagonal bond integrals are set to zero, but the electrostatic energy of solvation interaction between X^- and X assumes a non-zero value. Both eigenvalues of \mathbf{H} in Eq. (7) are equal to $\alpha + \sigma_{1,1}$. The corresponding eigenvectors, (1, 0) and (0, 1), describe the degenerate X^-X and $X\cdot X^-$ states of the cluster, each with a VSE = $-\sigma_{1,1}$ (Table 1).

4.2 Trimer anions of closed-shell molecules (n = 3)

 X_3 ⁻: Covalent trimer anions (n = 3, k = 3). We will consider two different X_3 ⁻ structures. The first is an [X-X-X]⁻ chain or stacked anion with a distinct central moiety, bound to two equivalent end moieties. Such structures have been proposed for π-stacked trimer anions of organic molecules, e.g., tetrachloroquinone⁶⁹ and biacetyl.⁵ We will investigate a similar (so far hypothetical) structure for glyoxal. Due to the geometric constraints, such a structure is unlikely for $(CO_2)_3$ ⁻. Other systems may seem to be plausible candidates for such covalent trimers, but form X_2 ⁻·X structures instead. We will also consider a triangular X_3 ⁻ structure, in which all three moieties are equivalent. Such a trimer can be envisaged for CO_2 , but it is less stable than the $(CO_2)_2$ ⁻·CO₂. The recently reported $(CO_3)_3$ ⁻ trimer⁷⁰ is an actual example of a triangular structure, with a caveat that under our classification it is a type-III (not type-I) species.

A triple-decker [X-X-X]⁻ structure has two IM bonds of an order of 1/4 each. (We will continue to use nominal Lewis-style bond orders, rather than those calculated from the eigenvector coefficients in the Hückel theory.⁷¹) The IM bonding in this structure is due to population of the bonding trimer IMO (which

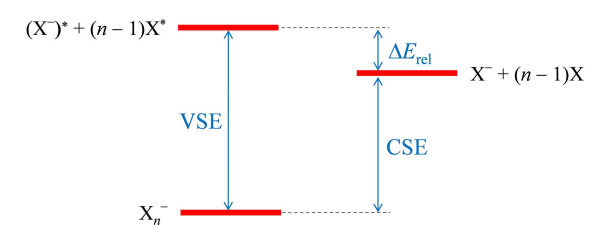


Fig. 5. Illustration of the vertical stabilisation energy (VSE), monomer relaxation energy, $\Delta E_{\rm rel}$, and adiabatic cluster stabilisation energy (CSE). X_n^-, X^- , and X are the relaxed structures. (X⁻)* and X* are the non-interacting monomers constrained to their internal geometries within the cluster.

is empty in the neutral state) by a single electron. The resulting order-of-1/2 bonding character is distributed between the two equivalent X-X bonds, yielding a nominal bond order (BO) of 1/4 for each. The trimer IMOs for glyoxal and biacetyl are shown in Fig. 4. Similar to the dimer (Sec. 4.1), the IM bonding in the stacked trimer results from a bonding overlap of the MMOs: $\phi = \sum c_i \psi_i$, where ψ_i are the LUMMOs of the neutral monomers, $\psi_{\text{LUMMO}}^{(i)}$ (i = 1 - 3), and ϕ is the trimer IMO. The Hückel-style Hamiltonian matrix for the [X-X-X]⁻ structure has the form:

$$\mathbf{H} = \begin{pmatrix} \alpha & \beta_{1/4} & 0 \\ \beta_{1/4} & \alpha & \beta_{1/4} \\ 0 & \beta_{1/4} & \alpha \end{pmatrix}$$
(8)

The Coulomb integrals α in Eq. (8) are the same as in other cases, depending only on the nature of X, but the bond integrals are distinct. As indicated by the subscript, $\beta_{1/4}$ in Eq. (8) corresponds to a 1/4-bond, while $\beta_{1/2}$ in Eq. (6) to a 1/2-bond. The use of the bond orders as labels does not imply that the integrals depend explicitly on BO; they do not. The bond order is a secondary construct, determined by the populations of the IMOs arising from the diagonalisation of the Hamiltonian. As in the conventional Hückel theory, the same H can describe systems with different bond orders, depending on the number of electrons. That said, the integrals $\beta_{BO} = \langle \psi_i | \hat{H} | \psi_j \rangle$, $i \neq j$, where $\{\psi_i\}$ is the MMO basis, do depend on the MMO overlap and, therefore, the IM separation, which in turn depends on the BO. One might say that $\partial \beta_{BO}/\partial (BO) = 0$, but $d\beta_{BO}/d(BO) \neq 0$. As bond length generally increases with decreasing BO, the smaller the BO, the smaller we expect $|\beta_{BO}|$ to be. Specifically, $|\beta_{1/4}| < |\beta_{1/2}|$.

The eigenvalues of **H** in Eq. (8) are (in increasing order): $\alpha + \sqrt{2}\beta_{1/4}$, α , and $\alpha - \sqrt{2}\beta_{1/4}$. Only the lowest-energy IMO will be populated by an electron, yielding two 1/4-IM bonds. The interaction energy, reflecting the combined energy of these two bonds, is VSE = $-\sqrt{2}\beta_{1/4}$ (Table 1). If $\beta_{1/4}$ and $\beta_{1/2}$ were equal, this would represent a 40% increase compared to the dimer anion. Since $|\beta_{1/4}| < |\beta_{1/2}|$, the additional stabilisation of [X-X-X]⁻, compared to [X-X]⁻, is smaller than that.

The normalized eigenvector corresponding to the bonding IMO given by Eq. (8) is $(1/2, 1/\sqrt{2}, 1/2)$. Assuming that all other electrons in the trimer are not affected, the partial charges of the monomers in $[X-X-X]^-$ are hence predicted to be -0.25, -0.50, and -0.25. In comparison, the overall Mulliken charges on the monomers in the triple-decker $(ba)_3^-$ structure shown in Fig. 4 are -0.285, -0.43, and -0.285, 5 but further discussion will follow in Sec. 5 about the validity of this comparison.

[§] Stacked (triple- and tetra-decker) structures are assumed for the k = 3 and 4 anions, respectively.

In a cyclic X_3^- structure, all three X moieties are presumed equivalent and each of the three IM bonds has an order of 1/6. This BO value reflects the sharing of the order-of-1/2 bonding character, attributed to a single electron in the lowest-energy IMO, between three equivalent IM bonds. The Hückel-style Hamiltonian matrix in this case has the form:

$$\mathbf{H} = \begin{pmatrix} \alpha & \beta_{1/6} & \beta_{1/6} \\ \beta_{1/6} & \alpha & \beta_{1/6} \\ \beta_{1/6} & \beta_{1/6} & \alpha \end{pmatrix}$$
(9)

Based on the above arguments, $|\beta_{1/6}| < |\beta_{1/4}| < |\beta_{1/2}|$. The eigenvalues for matrix (9) are $E_1 = \alpha + 2\beta$ and $E_{2,3} = \alpha - \beta$. Population of the lowest IMO by one electron results in a VSE = $-2\beta_{1/6}$. Since the cyclic core structures will not be discussed further, this result is not included in Table 1.

 X_2 -X or X_2 -X-: Covalent dimer anion solvated by one monomer (n = 3, k = 2) vs. Monomer anion solvated by two monomers (n = 3, k = 1). The Hückel-style Hamiltonian matrix describing both situations has a block-diagonal form:

$$\mathbf{H} = \begin{pmatrix} \alpha + \sigma_{2,1} & \beta_{1/2} & 0\\ \beta_{1/2} & \alpha + \sigma_{2,1} & 0\\ 0 & 0 & \alpha + \sigma_{1,2} \end{pmatrix}$$
(10)

The first 2×2 block corresponds to the covalently bound dimer, described by Eq. (6), now additionally solvated by one neutral X moiety, as described by $\sigma_{2,1}$. The second block, comprised of a single element $\alpha + \sigma_{1,2}$, represents an X^- moiety, not participating in IM bonding, but stabilised by two solvent monomers. Correspondingly, the first two eigenvalues of Eq. (10) describe an $X_2^-\cdot X$ structure, with the charge shared between the two X moieties within the dimer. The third solution describes an $X_2\cdot X^-$ (or $X^-\cdot X_2$) cluster, with the charge localised on one X moiety. Hence, the solvation factors are not the same within the two blocks: $\sigma_{2,1}$ represents the stabilisation of X_2^- by one neutral X moiety, while $\sigma_{1,2}$ describes the solvation of X^- by two neutral X. Hence, we expect $|\sigma_{2,1}| < |\sigma_{1,2}|$.

The eigenvalues of (10) are $E_1 = \alpha + \beta_{1/2} + \sigma_{2,1}$, $E_2 = \alpha - \beta_{1/2} + \sigma_{2,1}$, and $E_3 = \alpha + \sigma_{1,2}$. Their order depends on the relative magnitudes of $\beta_{1/2}$ and $(\sigma_{1,2} - \sigma_{2,1})$. If covalent bonding exceeds the solvation differential, $|\beta_{1/2}| > |\sigma_{1,2} - \sigma_{2,1}|$, E_1 is the lowest eigenvalue and the X_2^-X structure is preferred. The corresponding VSE is $-(\beta_{1/2} + \sigma_{2,1})$. If the covalent bonding is weaker than the solvation differential, E_3 is the lowest eigenvalue, indicating that it is more favourable for the charge to localise of one monomer and for the cluster to adopt the X^-X_2 configuration. The corresponding VSE is $-\sigma_{1,2}$ (Table 1).

4.3 Tetramer anions of closed-shell molecules (n = 4)

X4⁻: Purely covalent tetra-decker anion (n = 4, k = 4). There are three IM bonds in the [X1-X2-X3-X4]⁻ structure. By symmetry, X1-X2 and X3-X4 are equivalent, but X2-X3 is distinct. We will assume, as in the conventional Hückel theory, that all bond integrals are the same. Then, one bonding electron shared among these three bonds result in a 1/6 bond order for each. All IM interactions in this case are covalent, so there are no solvation elements in the Hückel-style Hamiltonian matrix:

$$\mathbf{H} = \begin{pmatrix} \alpha & \beta_{1/6} & 0 & 0\\ \beta_{1/6} & \alpha & \beta_{1/6} & 0\\ 0 & \beta_{1/6} & \alpha & \beta_{1/6}\\ 0 & 0 & \beta_{1/6} & \alpha \end{pmatrix}$$
(11)

The four eigenvalues are $E_{1-4}=\alpha\pm\beta_{1/6}$ ($\sqrt{5}\pm1$)/2, with $E_{1}=\alpha+\beta_{1/6}$ ($\sqrt{5}\pm1$)/2 being the lowest. Population of this IMO by an electron results in the three 1/6-bonds with a combined VSE = $-\beta_{1/6}$ ($\sqrt{5}\pm1$)/2 $\approx -1.62\beta_{1/6}$ (Table 1). The normalised eigenvector is $(1,(\sqrt{5}\pm1)/2,(\sqrt{5}\pm1)/2,1)/\sqrt{5}\pm\sqrt{5}$, which evaluates to (0.372, 0.602, 0.602, 0.372) and translates into the -0.14, -0.36, -0.36, -0.14 monomer charges.

 X_3 -X or X_3 -X⁻: Triple-decker anion solvated by one monomer (n = 4, k = 3) vs. Monomer-anion solvated by three monomers (n = 4, k = 1). Expanding on Eq. (10), the Hamiltonian matrix for such species is written as:

$$\mathbf{H} = \begin{pmatrix} \alpha + \sigma_{3,1} & \beta_{1/4} & 0 & 0\\ \beta_{1/4} & \alpha + \sigma_{3,1} & \beta_{1/4} & 0\\ 0 & \beta_{1/4} & \alpha + \sigma_{3,1} & 0\\ 0 & 0 & 0 & \alpha + \sigma_{1,3} \end{pmatrix}$$
(12)

Following the above arguments, $|\sigma_{3,1}| < |\sigma_{1,3}|$. The eigenvalues of matrix (12) are $E_1 = \alpha + \sqrt{2}\beta_{1/4} + \sigma_{3,1}$, $E_2 = \alpha + \sigma_{3,1}$, $E_3 = \alpha - \sqrt{2}\beta_{1/4} + \sigma_{3,1}$, and $E_4 = \alpha + \sigma_{1,3}$. Which is the lowest depends on the relative magnitudes of the bond integral $\beta_{1/4}$ and solvation differential $(\sigma_{1,3} - \sigma_{3,1})$. If $|\beta_{1/4}| > |\sigma_{1,3} - \sigma_{3,1}|/\sqrt{2}$, then E_1 is the lowest eigenvalue, corresponding to an X_3 -X structure with VSE = $-(\sqrt{2}\beta_{1/4} + \sigma_{3,1})$ (Table 1). On the other hand, if $|\beta_{1/4}| < |\sigma_{1,3} - \sigma_{3,1}|/\sqrt{2}$, E_4 is the lowest eigenvalue, corresponding to an X_3 -X-structure with VSE = $-\sigma_{1,3}$.

 $X_2 \overline{\ \ } X_2$: Covalent dimer anion solvated by two monomers (n = 4, k = 2). The Hamiltonian matrix for such species has a block-diagonal form:

$$\mathbf{H} = \begin{pmatrix} \alpha + \sigma_{2,2} & \beta_{1/2} & 0 & 0\\ \beta_{1/2} & \alpha + \sigma_{2,2} & 0 & 0\\ 0 & 0 & \alpha + \sigma_{1,3} & 0\\ 0 & 0 & 0 & \alpha + \sigma_{1,3} \end{pmatrix}$$
(13)

with the expectation that $|\sigma_{2,2}|<|\sigma_{1,3}|$. The eigenvalues for Eq. (13) are $E_1=\alpha+\beta_{1/2}+\sigma_{2,2}, E_2==\alpha-\beta_{1/2}+\sigma_{2,2}, E_{3,4}=\alpha+\sigma_{1,3}$. If $|\beta_{1/2}|>|\sigma_{1,3}-\sigma_{2,2}|$, then E_1 is the lowest and the preferred cluster structure is $X_2^-X_2$, with a VSE $=-(\beta_{1/2}+\sigma_{2,2})$ (Table 1). If, on the other hand, $|\beta_{1/2}|<|\sigma_{1,3}-\sigma_{2,2}|$, $E_{3,4}$ is the lowest (degenerate) eigenvalue, corresponding to an $X_3\cdot X^-(X_2\cdot X^-X$ or $X_2\cdot X\cdot X^-$) cluster structure with a VSE $=-\sigma_{1,3}$.

5 Examples and discussion

The CMMO formalism in Sec. 4 provides a simplified description of IM bonding in clusters with monomer and type-I polymer core anions. While not precise, the model offers a tutorial advantage over full-scale calculations by providing a simple and transparent picture of the IM interactions.

The model assumes either purely covalent or purely electrostatic interactions between certain pairs or groups of monomers.

In this section, we compare the model predictions to the properties of the glyoxal and biacetyl cluster anions determined using the density functional theory (DFT). In Sec. 5.1, we elaborate on the relevant properties of the $(gl)_n^-$ and $(ba)_n^-$, n=2-4 stacked structures shown in Fig. 4. The DFT structures are calculated without *a priori* assumptions about the IM interactions character and are best described by resonant combinations of covalent bonding and electrostatic solvation, optimised in each case to minimise the overall energy of the cluster. Comparing the DFT results to the baseline CMMO predictions is then used to assess the IM bonding character in these clusters, as well as to quantify the parameters appearing in the CMMO model. In Sec. 5.2, we apply the DFT and CMMO model results to the problem of electrostatic solvation obstructing covalent polymerisation.

5.1 DFT structures of glyoxal and biacetyl cluster anions

An overview of the stacked $(gl)_n^-$ and $(ba)_n^-$, n=1-4, structures is shown in Fig. 4; their complete geometric details are given in Electronic Supplementary Information. These structures were optimised in QChem $5.1,^{72}$ using the Minnesota-06 (M06-2X) functional, chosen for its performance on delocalised systems with non-covalent interactions.⁷³ All calculations employed Dunning's augmented correlation-consistent basis set of double-zeta quality (aug-cc-pVDZ).

The calculations included in this section are meant to create a semi-quantitative framework to support the CMMO model. Choosing a rigorously quantitative method to describe cluster anions requires extensive benchmarking beyond the objective of this work. Hence, except for gl⁻, ba⁻, (ba)₂⁻, and (ba)₃⁻, the structures in Fig. 4 do not necessarily correspond to global potential minima. Even if they do, they are not necessarily unique when it comes to the experiment. For example, the (ba)3- structure shown in the figure was identified as the global minimum for this cluster,5 but there are several solvated structures, described as (ba)2-ba, which are nearly degenerate with the triple-decker anion. The structures in Fig. 4 were optimised under the following symmetry constraints: D_2 for $(gl)_2^-$, C_2 for $(ba)_2^-$, C_{2h} for both (gl)₃⁻ and (ba)₃⁻, D₂ for (gl)₄⁻, and S₄ for (ba)₄⁻. Complete geometric surveys were not attempted, because they are expensive and, given our objective, unnecessary. Rather than proven global minima, these structures should be viewed as plausible geometries maximizing the IM π stacking interactions. As the best-case

scenarios for such interactions, these structures can be used to show that even under most favourable conditions, anionic polymerisation is still hindered by electrostatic solvation.

The CMMO solutions in Sec. 4 assume either purely covalent (β_{BO}) or purely electrostatic $(\sigma_{k,n-k})$ interactions within pairs or groups of monomers. Specifically, the stacked $(X)_n$, n = 2, 3, and 4 clusters, described by Eqs. (6), (8), and (11), respectively, are the limiting cases of purely covalent IM interactions. The corresponding charge distributions, determined in Sec. 4, are summarised in the CMMO column of Table 2. Eqs. (7), (9), (12), and (13), on the other hand, describe monomer, dimer, or trimer core anions solvated by neutral species. In real cluster structures, the bonding may fall in between the extremes of purely covalent and purely electrostatic forces. In general, each IM interaction within a cluster should be viewed as a coherent superposition of covalent bonding and electrostatic solvation, as represented, for example, by an $[X-X]^- \leftrightarrow X^- \cdot X$ resonance. We will use the calculated (DFT) structures and their charge distributions to assess the corresponding interaction characters.

The D_2 symmetry constraint in the (gl)₂⁻ calculation (Fig. 4) requires a -0.50/-0.50 charge sharing, as also predicted for a covalently bound X_2 ⁻ structure by Eq. (6). Relaxing the constraint leads to several less-favourable ion-molecule structures (not shown). In the analogous (ba)₂⁻ structure (C_2 symmetry), the two ba moieties are not equivalent, due to their different geometric motifs,⁵ but the charge remains significantly delocalised. Formally an $[X-X]^- \leftrightarrow X^- \cdot X$ resonance, the (ba)₂⁻ cluster in Fig. 4 retains a dominant $[X-X]^-$ covalent character. The larger IM separation in (ba)₂⁻ compared to (gl)₂⁻ (2.89 vs. 2.61 Å, Fig. 4) is attributed mostly to the bulky methyl groups in the former.

For $(gl)_3^-$ and $(ba)_3^-$ (Fig. 4), the C_{2h} symmetry constraint is satisfied by any superposition of two CMMO solutions: the purely covalent trimer anion $[X-X-X]^-$, described by the lowest eigenvalue of Eq. (8), and a twice-solvated monomer anion $X \cdot X^- \cdot X$, corresponding to the third solution of Eq. (10). The increased IM distances in $(gl)_3^-$ and $(ba)_3^-$, compared to the respective dimers, are consistent with the decreased IM bond orders (1/4 vs. 1/2, per Sec. 4) and the partial solvated characters. As will be discussed later, the monomer charges in the DFT structures, indeed reflect a mixture of the two bonding types.

Similarly, the D_2 and S_4 symmetry constraints of the respective (gl)₄ and (ba)₄ structures in Fig. 4 require the equivalences

Table 2. Partial charges on the individual moieties in the stacked double-, triple-, tetra-decker cluster structures calculated using the methods indicated.

Stacked			X = Glyoxal			X = Biacetyl			
Cluster	Moiety*	CMMO	Mulliken	Hirshfeld	Hirshfeld-I	Mulliken	Hirshfeld	Hirshfeld-I	
X_{2}^{-}	X1	-0.50	-0.50	-0.50	-0.50	-0.51	-0.60	-0.61	
	X2	-0.50	-0.50	-0.50	-0.50	-0.49	-0.40	-0.39	
X ₃ ⁻	X1	-0.25	0.02	-0.19	-0.15	-0.29	-0.20	-0.17	
	X2	-0.50	-1.04	-0.63	-0.69	-0.43	-0.59	-0.65	
	X3	-0.25	0.02	-0.19	-0.15	-0.29	-0.20	-0.17	
X ₄ ⁻	X1	-0.14	0.07	-0.09	-0.05	-0.23	-0.13	-0.10	
	X2	-0.36	-0.57	-0.41	-0.45	-0.27	-0.37	-0.40	
	X3	-0.36	-0.57	-0.41	-0.45	-0.27	-0.37	-0.40	
	X4	-0.14	0.07	-0.09	-0.05	-0.23	-0.13	-0.10	

^{*} The monomer moieties in the stacked structures are numbered sequentially: $X_2 = [X1-X2]^-$, $X_3 = [X1-X2-X3]^-$, and $X_4 = [X1-X2-X3-X4]^-$.

of the two terminal and the two inner moieties in each case. This restriction is satisfied by any combination of two CMMO solutions: the covalent tetramer anion [X·X-X-X]⁻, described by the lowest eigenvalue of Eq. (11), and the twice-solvated dimer structure X·[X-X]-X, described by Eq. (13). Comparing the (gl)₄ structure in Fig. 4 to (gl)₂, it is clear that (gl)₄ is predominantly a covalent dimer anion, solvated by two nearly neutral monomers: $X1 \cdot [X2-X3]^- \cdot X4$. Indeed, the separation between the two inner moieties (X2 and X3) in the tetramer is nearly identical to the IM distance in the dimer (2.62 vs. 2.61 Å). The X1-X2 and X3-X4 separations, on the other hand, are significantly larger, characteristic of solvation interactions. The slight difference between X2-X3 in (gl)₄ and the X-X distance in (gl)₂, as well as the slight charge delocalisation to the terminal moieties in the tetramer (discussed below) suggest some degree of $X \cdot [X-X]^{-} \cdot X$ \leftrightarrow [X·X-X-X]⁻ mixing, but the twice-solvated-dimer structure clearly dominates. A similar conclusion can be drawn about the (ba)₄ structure in Fig. 4, but allowing for a larger, compared to (gl)₄-, contribution of the covalent character. These conclusions about (gl)₄ and (ba)₄ are clearly supported by the appearance of their IMOs, which are predominantly localised on the two inner monomer moieties in both cases (see Fig. 4).

We now turn to the quantitative evaluation of the partial charges of the monomers. These charges (summed over all atoms in each moiety) for the $(gl)_n^-$ and $(ba)_n^-$, n=2-4 DFT structures are listed in Table 2 alongside the CMMO benchmarks. Three types of charges from the DFT calculations are included: those based on the Mulliken population analysis, ⁷⁴ the Hirshfeld charges, ⁷⁵ and those determined using the iterative Hirshfeld procedure (Hirshfeld-I). ^{76,77} The Mulliken and Hirshfeld-I charges were obtained directly in QChem. ⁷² The standard Hirshfeld charges (not available in QChem for charged molecules) were obtained from the QChem checkpoint files using the Multiwfn wavefunction analyser with build-in atomic densities. ⁷⁸

The need for a thoughtful examination of the different methods is evidenced by their divergent results. The Mulliken charges are strongly dependent on the choice of basis set, 79 which makes their use in our analysis problematic; they are included in Table 2 only as a commonly used reference. For example, qualitatively different Mulliken charge distributions are obtained for the (gl)₃vs. (ba)₃-: X·X-X vs. [X-X-X]-, respectively. Similarly, a partially zwitterionic, twice-solvated-dimer-anion structure X·X₂-·X is indicated for (gl)₄- (Mulliken charges: +0.07/-0.57/ -0.57/+0.07), compared to the strongly delocalised (even more so than the CMMO prediction) [X-X-X-X] structure of (ba)4-(-0.23/-0.27/-0.27/-0.23). Such significant disparity in the glyoxal vs. biacetyl cluster properties of is not supported by an indepth review, including the IMO properties in Fig. 4, or by other, more reliable types of charges. In contrast to the Mulliken population analysis, Hirshfeld charges are known to be nearly independent of the basis set choice and have linear relationships with chemical properties, such as carbon hybridisation and acidity.⁷⁹ Between the Hirshfeld and Hirshfeld-I charges included in Table 2, the latter are most appropriate for charged systems. ^{76,77} They are indicated for each monomer moiety in Fig. 4 and the following discussion will focus exclusively on them.

As already mentioned, the charge in the D_2 symmetry $(gl)_2^-$

structure (Fig. 4) is shared equally between the equivalent gl moieties. It remains significantly delocalised (60/40%) in (ba)2⁻, in which the two ba moieties are not equivalent. This result is consistent with the predominantly covalent nature of the IM interactions in (ba)2⁻: the CMMO model would describe it by assigning the first ba moiety a slighter greater magnitude of the Coulomb integral in Eq. (6).

In the trimers, the Hirshfeld-I charge on the central moiety is -0.69 for $(gl)_3^-$ and -0.65 for $(ba)_3^-$, each larger in magnitude than -0.50 predicted for a purely covalent trimer by CMMO, but smaller than -1 corresponding to an $X \cdot X^- \cdot X$ structure. These Hirshfeld-I charges suggest truly mixed $[X-X-X]^- \leftrightarrow X \cdot X^- \cdot X$ characters of both $(gl)_3^-$ and $(ba)_3^-$, with the weight of $[X-X-X]^-$ being larger in $(ba)_3^-$, compared to $(gl)_3^-$. These conclusions are consistent with the geometric structures.

The (gl)₄⁻ and (ba)₄⁻ structures have the -0.05/-0.45/-0.45/-0.45/-0.05 and -0.10/-0.40/-0.40/-0.10 Hirshfeld-I charge distributions, respectively, compared to the purely covalent -0.14/-0.36/-0.36/-0.14 CMMO benchmark. As in the trimer case, the tetramers should be viewed as superpositions of the covalent [X-X-X-X]⁻ and solvated $X \cdot [X-X]^- \times IM$ characters, with the covalent share again being greater in (ba)₄⁻, compared to (gl)₄⁻. Again, these conclusions are consistent with the bonding characters derived earlier in this section from the geometric structures.

The energetics of IM interactions is most logically quantified using the cluster stabilization energy, CSE, defined as the difference between the relaxed $X^- + (n-1)X$ dissociation limit and the $(X)_n^-$ cluster (Fig. 5). For comparison with the CMMO model, we will also consider each cluster's vertical stabilisation energy, VSE, defined as the energy of all IM interactions, excluding the internal relaxation energy of the monomers, $\Delta E_{\rm rel}$. VSE is calculated as the difference between the system of non-interacting monomers, $(X^-)^* + (n-1)X^*$, and the X_n^- cluster, where the energy of each asterisked X^-/X moiety is calculated at its geometry within the optimised cluster structure. As shown in Fig. 5, CSE = VSE – $\Delta E_{\rm rel}$.

Since charge sharing is an interaction, in determining the $(X^-)^* + (n-1)X^*$ energy in the absence of IM interactions, the excess electron must be placed on a specific X moiety, making VSE dependent on this choice. The logical choice is the monomer with the largest partial charge within the cluster. For example, in the stacked X_3^- structure, the middle X moiety becomes X^- . In $(gl)_2^-$, on the other hand, the two gl moieties are equivalent, so it does not matter which one is assigned the charge in the $gl+gl^-$ limit. In $(ba)_2^-$, the top ba moiety in Fig. 4 carries a larger fraction of the charge, and so it is this moiety that is treated as ba^- in the VSE calculation.

When CSE and VSE are determined from the $(X)_n^-$, X^- , and X energies calculated separately, the results overestimate the cluster stability due to the basis set superposition error (BSSE): the effect of using n times as many basis functions for the X_n^- cluster than for the individual X and X^- fragments. Although the BSSE is often ignored, it can be significant, especially for weak interactions. To minimise its effect, we determined the energies of all monomers frozen at their respective cluster geometries, using the same basis as that used for the entire cluster (the counterpoise correction). For each monomer, the atoms of all other

Table 3. Stacked cluster ener	getics from the M06-2X/aug-	cc-pVDZ calculations. All values are in elec	ctron-volts.*,§

		X = Glyoxal		X = Biacetyl			
Cluster	VSE (a) / (b) Relaxation		CSE (a) / (b)	VSE (a) / (b)	Relaxation	CSE (a) / (b)	
X_{2}^{-}	1.137 / 1.088	0.296	0.842 / 0.792	1.109 / 1.020	0.157	0.952 / 0.863	
X ₃ -	1.404 / 1.324	0.151	1.253 / 1.173	1.758 / 1.583	0.088	1.670 / 1.495	
X_4^-	1.976 / 1.800	0.385	1.591 / 1.415	2.432 / 2.159	0.428	2.005 / 1.731	

^{*} The stacked double- triple-, and tetra-decker structures shown in Fig. 4 are assumed for the n = 2, 3 and 4 anions, respectively.

moieties were replaced with ghost atoms in the same positions, allowing the calculation to be carried out without the extraneous moieties, but with their basis functions in place. That is, the energies of all X and X^- building blocks and the intact cluster X_n^- were determined using identical basis sets, with the same numbers of basis functions. Table 3 lists the VSE values calculated using two approaches: (a) the conventional method, involving the calculation of the X_n^- , X, and X^- energies in the respective basis sets without the BSSE correction; and (b) the ghost-atom method described above, which corrects for the BSSE. As seen in the table, the conventional calculations overestimate the interactions by 0.1-0.3 eV, depending on the cluster.

Next, the relaxation energy, $\Delta E_{\rm rel}$, was determined for each cluster. The contribution of each monomer was calculated as the energy difference between the monomer's structure within the cluster and its relaxed geometry. The overall relaxation energies (summed over all building blocks) for $(gl)_n^-$ and $(ba)_n^-$, n = 2-4are summarised in Table 3. The smaller ΔE_{rel} values for n = 3, compared to n = 2 and 4 confirms the significant contributions of the X·X-X character to the trimer structures. As expected, the relaxation energy is larger in the presence of covalent IM forces, as in the n = 2 cases. Subtracting ΔE_{rel} from VSE gives CSE (Fig. 5). Note that the CSE(a) values determined as CSE = VSE – ΔE_{rel} without the BSSE correction are identical to those obtained by the conventional method of subtracting the $(X)_{n}$ energy from the relaxed $X^- + (n-1)X$ limit, with all species examined using their respective differently-sized basis sets. In the following discussion, we will use the corrected VSE and CSE values (b).

5.2 How solvation obstructs polymerisation

In Sec. 5.1, we concluded that IM interactions in a cluster are generally admixtures of covalent and noncovalent forces. This is not to say that some moieties may be bound to each other by covalent bonds, while others by solvation (this is a given). What it means is that *each* IM interaction may include covalent and non-covalent components. The $[X-X-X]^- \leftrightarrow X \cdot X^- \cdot X$ resonance mentioned in Sec. 5.1 is one example. In contrast, the CMMO model (Sec. 4) categorises each interaction as either covalent

(described by β_{BO}) or non-covalent ($\sigma_{k,n-k}$). It thus describes benchmark structures for constructing the coherent combinations to describe the true, mixed interactions. Our next step is to evaluate the relative stabilities of the benchmark CMMO structures. In this section, we enumerate the CMMO results, summarised in Table 1, using the reasonable values of the bond integrals and solvation factors, determined using the DFT results in Sec. 5.1.

The CMMO parameter values assumed in the following analysis are summarised in Table 4. They were determined as described below, using the energetics in Table 3. First, based on the (gl)₂⁻ and (ba)₂⁻ VSE values, 1.0-1.1 eV is assumed to be the strength of a 1/2-IM bond in such systems, corresponding to $|\beta_{1/2}|$. Recall also that the 1/4-bond and 1/6-bond integrals should be smaller in magnitude: $|\beta_{1/2}| > |\beta_{1/4}| > |\beta_{1/6}|$. As discussed in Sec. 4.2, this trend is due to the larger separations between the monomers bound by weaker bonds, rather than a direct consequence of reduced bond orders. A quantitative insight into this trend is glimpsed from the DFT results. First, comparing the $(gl)_2^-$ and $(ba)_2^-$ structures (with similar $\pi - \pi$ interactions), the slight difference between VSE = 1.088 eV for (gl)2⁻¹ and VSE = 1.020 eV for $(ba)_2$ (Table 3) is attributed to the different IM separations: 2.61 vs. 2.89 Å (Fig. 4). This corresponds to a 0.068 eV drop in $|\beta_{BO}|$ per 0.28 Å separation increase. Since the IM distance in (gl)₃⁻ is 0.19 Å larger than in (gl)₂⁻ (Fig. 4), we project a 0.046 eV decrease in $|\beta_{BO}|$ for BO = 1/4 from BO = 1/2. Alternatively, we also calculated the $(gl)_2$ energy with the IM separation increased to 2.80 Å (which corresponds to a 1/4-IM bond), while freezing all other geometric parameters. This resulted in a 0.034 eV decrease in VSE. Averaging these results, we will assume a 0.04 eV drop in $|\beta_{BO}|$ from BO = 1/2 to 1/4, and similar from 1/4 to 1/6. In order not to repeat the same analysis for $(gl)_n^-$ and $(ba)_n^-$ and to make the discussion more general and easily amendable to other systems, we opt to express the model energetics in arbitrary units (a.u.), instead of electronvolts. Bringing it together, we set $\beta_{1/2} = -1.09$ a.u. $\beta_{1/4} = -1.05$ a.u. and $\beta_{1/6} = -1.01$ a.u. (Table 4).

There is more ambiguity about the solvation factors $\sigma_{k,n-k}$, but a combination of the DFT results and experimental values for

Table 4. CMMO model parameters used in Fig. 6, expressed in arbitrary energy units (intended to correspond approximately to electron-volts).

	$\beta_{1/2}$	$\beta_{1/4}$	$\beta_{1/6}$	$\sigma_{1,1}$	$\sigma_{1,2}$	$\sigma_{1,3}$	$\sigma_{2,1}$	$\sigma_{2,2}$	$\sigma_{3,1}$
Set I (weaker solvation)	-1.09	-1.05	-1.01	-0.40	-0.72	-1.00	-0.32	-0.56	-0.26
Set II (stronger solvation)	-1.09	-1.05	-1.01	-0.60	-1.08	-1.50	-0.48	-0.84	-0.40

[§] The (a) values of VSE and CSE were determined from the X_n^- , X_n^- and X^- energies calculated in the respective basis sets, with n times as many basis functions for X_n^- than for X or X^- . Therefore, these results suffer from the basis set superposition error. The (b) values correct for the BSSE by calculating the X_n^- , X_n^- , and X^- energies in the same (X_n^-) basis, as described in the text.

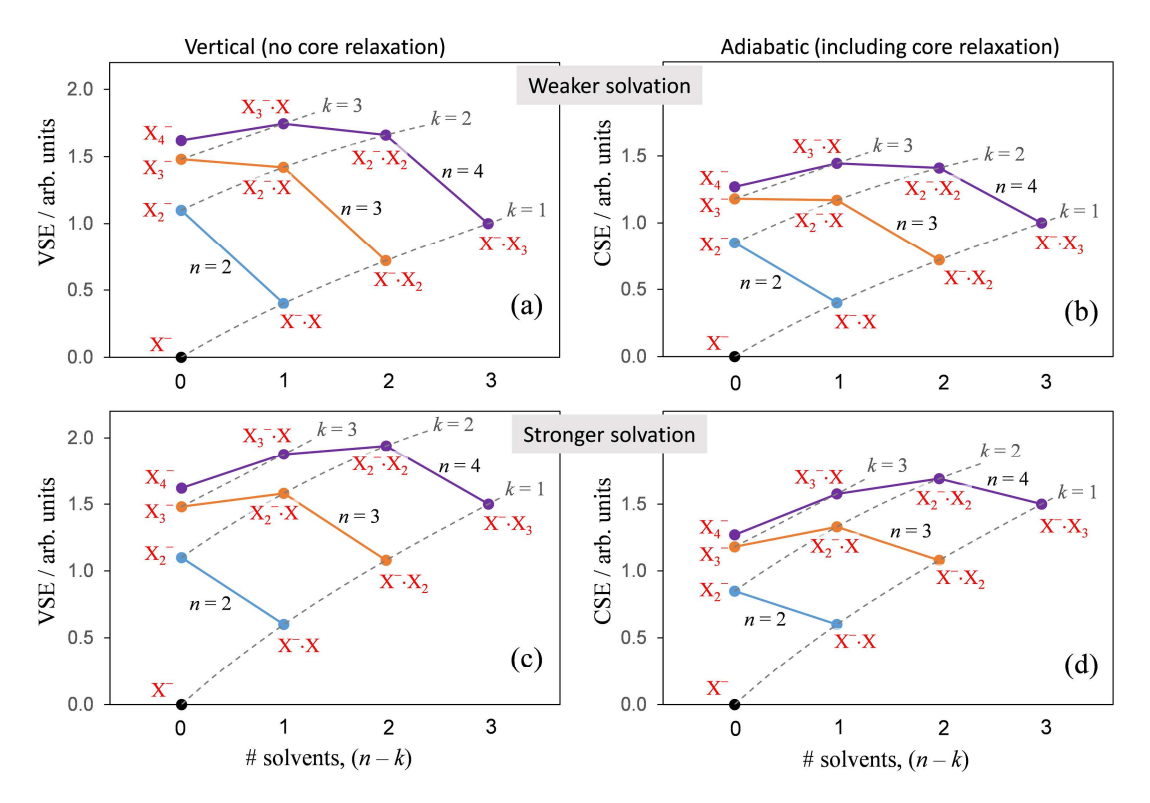


Fig. 6. Vertical (left) and adiabatic (right) stabilisation trends for various $X_k^- X_{n-k}$ clusters, predicted by the CMMO model with parameter sets I and II in Table 4, corresponding to relatively weak (top) and relatively strong (bottom) solvation regimes. The VSE and CSE values are plotted versus the number of neutral solvent monomers, (n-k). Solid lines n=2-4 represent clusters of the same size (n=const) with varying sizes of the core anion (k). Dashed lines k=1-3 describe stepwise solvation of a given core anion.

many cluster systems^{1,2} allows us to consider two solvation regimes, represented by sets I and II (Table 4). The two sets differ in solvation factors only. Set I is defined by a 0.4 a.u. stabilisation of the X⁻·X complex. Set II represents 50% stronger solvation, with a 0.6 a.u. X⁻·X stabilisation energy. All other solvation factors are scaled the same way. In each set, for the same core size (k), $\sigma_{k,n-k}$ increase in magnitude with the number of solvating monomers, (n-k). The increase is monotonic, but slower than linear, e.g., $|\sigma_{1,1}| < |\sigma_{1,2}| < |\sigma_{1,3}|$, but $|\sigma_{1,3} - \sigma_{1,2}| < |\sigma_{1,2} - \sigma_{1,1}| < |\sigma_{1,1}|$, as expected in stepwise solvation. On the other hand, increasing the core size k, while keeping the number of solvent molecules (n-k) constant, decreases the solvation energy, as discussed in Sec. 2: $|\sigma_{1,1}| > |\sigma_{2,1}| > |\sigma_{3,1}|$.

Using these parameters, we enumerate the IM interactions in the benchmark $X_k^- \cdot X_{n-k}$ clusters described by the CMMO model. The results are presented in Fig. 6, which displays the vertical and adiabatic stabilisation trends in the two regimes, plotted versus the number of solvent monomers, (n-k). (a) and (c) show the VSE values, calculated using the expressions from Table 1, with parameter sets I and II, respectively, from Table 4. Graphs (b) and (d) include the relaxation energies, with one more simplifying assumption: they neglect the relaxation of the neutral (solvent) moieties, accounting for the core anion contributions only. Guided by the DFT results in Table 3, the following core relaxation energies are assumed: 0.25 a.u. for the dimer, 0.30 a.u. for the trimer, and 0.35 a.u. for the tetramer. Note that the inclusion of core relaxation does not change the qualitative trends.

The structural formulas of the clusters are indicated next to each data point in Fig. 6. Note that the increase in the VSE/CSE values for the purely covalent X_{1-4} structures saturates quickly, as mentioned in Sec. 4. To help identify the observed trends, two types of trend lines are included in Fig. 6. Solid lines track clusters of the same size (n = const), but with varying core anions (k), e.g. X_3^- , $X_2^- \cdot X$, and $X^- \cdot X_2$. Dashed lines represent stepwise solvation of a given core anion (k = const), e.g. X^- , $X^- \cdot X$, $X^- \cdot X_2$, and X-X₃. The maximum of each solid curve represents the most stable form for that size n. In the relatively weak solvation regime (top half of Fig. 6), the most stable form of n = 2 clusters is the covalent dimer, X_2^- . For n = 3, it is the covalent trimer, X_3^- , while for n = 4, it is the mono-solvated trimer $X_3 \cdot X$. Thus, in this regime, the formation of covalently bound dimer and trimer anions is energetically feasible, but tetramer anions is not. In the case of stronger solvation (bottom half of Fig. 6), the picture changes. X_2^- , $X_2^- \cdot X$, and $X_2^- \cdot X_2$ are the most stable forms of the respective n = 2, 3, and 4 cluster anions. That is, of the covalent cluster cores, only the dimer, X₂-, is favoured by the energetics, while trimer and larger polymer anions are not expected to form.

Summarising the findings, the charge-sharing polymerisation beyond dimerisation is favourable energetically only if solvation is significantly weaker than IM covalent bonding. With stronger solvation, the polymerisation trend is truncated at the dimer stage. Extrapolating this trend, we predict that if the IM covalent interactions are weak relative to solvation, the monomer anion is expected to be the core for all cluster sizes. Again, the trends

shown in Fig. 6 are the CMMO model predictions for the cases of pure covalent or pure solvation interactions within each pair of monomers. The real clusters may involve admixtures of these basic bonding types. As for any resonance, the weights of the contributions are dependent on the relative stabilities of the ideal structures. We discussed these stabilities using the CMMO framework, with the results are summarised in Table 1. Figure 6 gives two examples of enumeration of these analytic results.

We should also consider the entropic contributions to cluster free energy. Entropy favours less-rigid structures and, therefore, smaller-sized cluster cores, creating an additional hurdle for anionic polymerisation. In cases when the stabilisation energies of, say, X_3^- and X_2^- :X are similar, as in both solvation regimes in Fig. 6, entropy will favour the solvated form of the cluster, because it corresponds to a larger accessible volume of the configuration space, compared to the more rigid and constrained covalent-anion structure. In a similar vein, the limits of electronic coherence due to vibronic couplings in large enough systems also favour charge localisation and smaller-sized cluster cores.

Conclusions

We discussed the formation of weak covalent bonds, responsible for anionic dimerisation and polymerisation in cluster environments. We outlined a new perspective on this problem, by introducing the coupled-monomers MO model, which relies on the first-order separability of inter- and intra-monomer interactions. The model offers an approximate description of the inter-monomer covalent bonding in terms of coherent charge sharing. A Hückel-style formalism, adapted specifically to weak covalent and solvation interactions in clusters, offers insight into the competition between these types of interactions. A quantitative analysis of the results suggests that under typical conditions in common cluster anions, the cumulative effect of solvation tends to limit the size of covalently bound cluster cores to monomer, dimer, and, in some cases, trimer anions. The stronger the solvation relative to covalent forces, the smaller the sizes of the core anions favoured by equilibrium thermodynamics.

Acknowledgements

We are grateful to Dr. Laura O. Van Dorn for comments on the manuscript. This work was supported by the U.S. National Science Foundation (grant CHE-1664732).

Conflicts of interest

There are no conflicts to declare.

Notes and references

- A. W. Castleman and K. H. Bowen, J. Phys. Chem., 1996, 100, 12911.
- A. Sanov and W. C. Lineberger, *Phys. Chem. Chem. Phys.*, 2004, 6, 2018.
- S. H. Fleischman and K. D. Jordan, J. Phys. Chem., 1987, 91, 1300.

- C. A. Hunter and J. K. M. Sanders, J. Am. Chem. Soc., 1990, 112, 5525.
- Y. Dauletyarov, A. A. Wallace, C. C. Blackstone and A. Sanov, J. Phys. Chem. A, 2019, 123, 4158.
- M. J. DeLuca, B. Niu and M. A. Johnson, J. Chem. Phys., 1988, 88, 5857.
- T. Tsukuda, M. A. Johnson and T. Nagata, Chem. Phys. Lett., 1997, 268, 429.
- 8. E. J. Hart and J. W. Boag, J. Am. Chem. Soc., 1962, 84, 4090.
- 9. M. Armbruster, H. Haberland and H. G. Schindler, *Phys. Rev. Lett.*, 1981, 47, 323.
- 10. J. Schnitker, K. Motakabbir, P. J. Rossky and R. Friesner, *Phys. Rev. Lett.*, 1988, **60**, 456.
- L. A. Posey, P. J. Campagnola, M. A. Johnson, G. H. Lee, J. G. Eaton and K. H. Bowen, *J. Chem. Phys.*, 1989, 91, 6536.
- L. A. Posey, M. J. DeLuca, P. J. Campagnola and M. A. Johnson, J. Phys. Chem., 1989, 93, 1178.
- 13. P. J. Campagnola, L. A. Posey and M. A. Johnson, *J. Chem. Phys.*, 1990, **92**, 3243.
- J. V. Coe, G. H. Lee, J. G. Eaton, S. T. Arnold, H. W. Sarkas, K. H. Bowen, C. Ludewigt, H. Haberland and D. R. Worsnop, J. Chem. Phys., 1990, 92, 3980.
- S. T. Arnold, R. A. Morris and A. A. Viggiano, J. Chem. Phys., 1995, 103, 9242.
- C. G. Bailey, J. Kim and M. A. Johnson, J. Phys. Chem., 1996, 100, 16782.
- 17. P. Ayotte and M. A. Johnson, J. Chem. Phys., 1997, 106, 811.
- J. Kim, I. Becker, O. Cheshnovsky and M. A. Johnson, *Chem. Phys. Lett.*, 1998, **297**, 90.
- O. P. Balaj, C. K. Siu, I. Balteanu, M. K. Beyer and V. E. Bondybey, *Chem-Eur J*, 2004, **10**, 4822.
- A. E. Bragg, J. R. R. Verlet, A. Kammrath, O. Cheshnovsky and D. M. Neumark, *Science*, 2004, 306, 669.
- K. R. Asmis, G. Santambrogio, J. Zhou, E. Garand, J. Headrick, D. Goebbert, M. A. Johnson and D. M. Neumark, J. Chem. Phys., 2007, 126.
- K. A. Hanold, C. R. Sherwood and R. E. Continetti, *J. Chem. Phys.*, 1995, 103, 9876.
- K. A. Hanold, M. C. Garner and R. E. Continetti, *Phys. Rev. Lett.*, 1996, 77, 3335.
- H. Hsieh and R. Quirk, Anionic Polymerization: Principles and practical applications, Marcel Dekker, New York, 1996.
- E. R. Grumbling, K. Pichugin, L. Velarde and A. Sanov, *J. Phys. Chem. A*, 2010, **114**, 1367.
- 26. T. Kondow and K. Mitsuke, J. Chem. Phys., 1985, 83, 2612.
- A. Sanov, S. Nandi, K. D. Jordan and W. C. Lineberger, *J. Chem. Phys.*, 1998, 109, 1264.
- T. Habteyes, L. Velarde and A. Sanov, J. Chem. Phys., 2009, 130, 124301.
- Y. Kobayashi, Y. Inokuchi and T. Ebata, J. Chem. Phys., 2008, 128, 164319.
- T. Habteyes, L. Velarde and A. Sanov, J. Phys. Chem. A, 2008, 112, 10134.
- 31. T. Habteyes and A. Sanov, *J. Chem. Phys.*, 2008, **129**, 244309
- L. A. Yu, A. H. Zeng, Q. A. Xu and M. F. Zhou, J. Phys. Chem. A, 2004, 108, 8264.
- R. Mabbs, E. Surber and A. Sanov, Chem. Phys. Lett., 2003, 381, 479.
- S. Koizumi, H. Yasumatsu, S. Otani and T. Kondow, *J. Phys. Chem. A*, 2002, **106**, 267.
- 35. S. W. Zhang, C. G. Zhang, Y. T. Yu, B. Z. Mao and F. C. He,
- Chem. Phys. Lett., 1999, 304, 265.
 36. A. Sanov, W. C. Lineberger and K. D. Jordan, J. Phys. Chem. A, 1998, 102, 2509.
- T. Maeyama, T. Oikawa, T. Tsumura and N. Mikami, J. Chem. Phys., 1998, 108, 1368.
- 38. T. Tsukuda, T. Hirose and T. Nagata, Chem. Phys. Lett., 1997,

- **279**, 179.
- K. Hiraoka, S. Fujimaki, G. Aruga and S. Yamabe, *J. Phys. Chem.*, 1994, 98, 1802.
- R. J. Li and R. E. Continetti, J. Phys. Chem. A, 2002, 106, 1183.
- 41. K. Pichugin, E. Grumbling, L. Velarde and A. Sanov, *J. Chem. Phys.*, 2008, **129**, 044311.
- 42. L. Velarde, T. Habteyes, E. R. Grumbling, K. Pichugin and A. Sanov, J. Chem. Phys., 2007, 127, 084302.
- I. Yourshaw, Y. X. Zhao and D. M. Neumark, J. Chem. Phys., 1996, 105, 351.
- M. Saeki, T. Tsukuda and T. Nagata, Chem. Phys. Lett., 2001, 348, 461.
- M. Saeki, T. Tsukuda and T. Nagata, Chem. Phys. Lett., 2001, 340, 376.
- R. Mabbs, E. Surber, L. Velarde and A. Sanov, J. Chem. Phys., 2004, 120, 5148.
- T. Tsukuda, M. Saeki, L. Zhu and T. Nagata, Chem. Phys. Lett., 1998, 295, 416.
- 48. L. A. Posey and M. A. Johnson, *J. Chem. Phys.*, 1988, **88**,
- 5383. 49. J. Hacaloglu, S. Suzer and L. Andrews, *J. Phys. Chem.*, 1990,
- 94, 1759. 50. M. E. Jacox and W. E. Thompson, *J. Chem. Phys.*, 1990, 93,
- 51. M. E. Jacox, J. Chem. Phys., 1990, 93, 7622.
- D. W. Arnold and D. M. Neumark, J. Chem. Phys., 1995, 102, 7035.
- D. L. Osborn, D. J. Leahy, D. R. Cyr and D. M. Neumark, *J. Chem. Phys.*, 1996, **104**, 5026.
- M. R. Nimlos, G. Davico, C. M. Geise, P. G. Wenthold, W. C. Lineberger, S. J. Blanksby, C. M. Hadad, G. A. Petersson and G. B. Ellison, *J. Chem. Phys.*, 2002, 117, 4323.
- M. J. DeLuca, C.-C. Han and M. A. Johnson, *J. Chem. Phys.*, 1990, 93, 268.
- C. R. Sherwood, K. A. Hanold, M. C. Garner, K. M. Strong and R. E. Continetti, *J. Chem. Phys.*, 1996, 105, 10803.
- 57. R. J. Li, K. A. Hanold, M. C. Garner, A. K. Luong and R. E. Continetti, *Faraday Discuss.*, 1997, **108**, 115.
- A. J. A. Aquino, P. R. Taylor and S. P. Walch, J. Chem. Phys., 2001, 114, 3010.
- D. J. Goebbert and A. Sanov, J. Chem. Phys., 2009, 131, 104308.
- D. Khuseynov, D. J. Goebbert and A. Sanov, J. Chem. Phys., 2012, 136, 094312.
- D. Khuseynov, A. R. Dixon, D. J. Dokuchitz and A. Sanov, J. Phys. Chem. A, 2014, 118, 4510.
- J. W. Shin, N. I. Hammer, M. A. Johnson, H. Schneider, A. Gloss and J. M. Weber, *J. Phys. Chem. A*, 2005, 109, 3146.
- K. B. Bravaya, B. L. Grigorenko, A. V. Nemukhin and A. I. Krylov, Acc. Chem. Res., 2012, 45, 265.
- C. S. Anstöter, C. R. Dean and J. R. R. Verlet, *Phys. Chem. Chem. Phys.*, 2017, 19, 29772.
- 65. P. A. Pieniazek, A. I. Krylov and S. E. Bradforth, *J. Chem.*
- *Phys.*, 2007, **127**, 044317.66. A. A. Golubeva and A. I. Krylov, *Phys. Chem. Chem. Phys.*,
- 2009, 11, 1303.K. B. Bravaya, O. Kostko, M. Ahmed and A. I. Krylov, *Phys.*
- Chem. Chem. Phys., 2010, 12, 2292.
- A. A. Wallace, Y. Dauletyarov and A. Sanov, *J. Phys. Chem.* A, 2021, 125, 317.
- K. Molcanov, Z. Y. Mou, M. Kertesz, B. Kojic-Prodic, D. Stalke, S. Demeshko, A. Santic and V. Stilinovic, *Chem-Eur J*, 2018, 24, 8292.
- B. Chen, D. A. Hrovat, R. West, S. H. M. Deng, X. B. Wang and W. T. Borden, *J. Am. Chem. Soc.*, 2014, 136, 12345.
- I. N. Levine, Quantum Chemistry, Prentice-Hall, Inc., Upper Saddle River, NJ, 2000.

- 72. Y. H. Shao, et al., Mol. Phys., 2015, 113, 184.
- Y. Zhao and D. G. Truhlar, Theor. Chem. Acc., 2008, 120, 215.
- 74. R. S. Mulliken, J. Chem. Phys., 1955, 23, 1833.
- 75. F. L. Hirshfeld, Theoretica Chimica Acta, 1977, 44, 129.
- 76. P. Bultinck, Faraday Discuss., 2007, 135, 347.
- P. Bultinck, C. V. Alsenoy, P. W. Ayers and R. Carbó-Dorca, J. Chem. Phys., 2007, 126, 144111.
- 78. T. Lu and F. Chen, J. Comput. Chem., 2012, 33, 580.
- K. B. Wiberg and P. R. Rablen, J. Org. Chem., 2018, 83, 15463.
- 80. S. F. Boys and F. Bernardi, Mol. Phys., 1970, 19, 553.